EVALUATION OF HEAT AND MASS TRANSFER MODELS FOR SIZING LOW TEMPERATURE KALINA CYCLE MICROCHANNEL CONDENSERS

Brian M. Fronk[1]
School of Mechanical, Industrial and Manufacturing Engineering
Oregon State University
204 Rogers Hall
Corvallis, OR 97331
Brian.Fronk@oregonstate.edu
ASME Member

Kyle R. Zada
School of Mechanical, Industrial and Manufacturing Engineering
Oregon State University
204 Rogers Hall
Corvallis, OR 97331
zadak@oregonstate.edu

Abstract

Waste heat driven ammonia/water Kalina cycles have shown promise for improving the efficiency of electricity production from low temperature reservoirs ($T < 150°C$). However, there has been limited application of these systems to utilize widely available, disperse, waste heat streams for smaller scale power production (1 to 10 kWe). Factors limiting increased deployment of these systems include large, costly heat exchangers, and concerns over safety of the working fluid. The use of mini and microchannel ($D < 1$ mm) heat exchangers has the potential to decrease system size and material cost, while also reducing the working fluid inventory, enabling penetration of Kalina cycles into these new markets.

However, accurate methods of predicting the heat and mass transfer in microscale geometries must be available to design and optimize these compact heat exchangers. In the present study, the effect of different heat and mass transfer models on the calculated Kalina cycle condenser size is investigated at representative system conditions. A detailed heat exchanger model for a liquid-coupled microchannel ammonia/water condenser is developed. The heat exchanger is sized using different predictive methods to provide the required heat transfer area for a 1 kWe Kalina system with a source and sink temperature of 150°C and 20°C, respectively. The results show that for the models considered, predicted heat exchanger size can vary by up to 58%. Based on prior experimental results, a non-equilibrium approach is recommended to provide the most accurate, economically sized ammonia/water condenser.

[1] Corresponding author: brian.fronk@oregonstate.edu ; +1-(541)-737-3952

NOMENCLATURE

A	area (m^2)
c_p	specific heat (kJ kg^{-1} K^{-1})
C	concentration (kmol m^{-3})
Ca_L	liquid capillary number $=\mu_L \cdot j_L / \sigma$
D	diameter (m)
G	mass flux (kg m^{-2} s^{-1})
g	gravitational acceleration (m s^{-2})
h	specific enthalpy (kJ kg^{-1})
j	superficial velocity (m s^{-1})
j_G^*	dimensionless gas velocity (-)
k	thermal conductivity (W m^{-1} K^{-1})
kWe	Kilowatt-electric
L	length (m)
LMTD	log-mean temperature difference (K)
$\dot{m}$	mass flow rate (kg s^{-1})
m''	condensing mass flux (kg m^{-2} s^{-1})
$\dot{N}$	condensing molar flux (kmol m^{-2} s^{-1})
Nu	Nusselt number (-)
P	pressure (kPa)
Pr	Prandtl number (-)
P_r	reduced pressure $=P/P_{crit}$
q	quality (-)
$\dot{Q}$	heat duty (kW)
R	thermal resistance (K W^{-1})
Re	Reynolds number (-)
$Re_{L,\varepsilon}$	film Reynolds number
Su_{VO}	vapor-only Suratman number $=\rho_V \cdot \sigma \cdot D / \mu_V^2$
T	temperature (°C)
t	thickness (mm)
U	velocity (m s^{-1})
$\bar{V}_{vj}$	vapor drift flux velocity (m s^{-1})
$\dot{W}_{net}$	net power (kW)
We^*	modified Weber number
x_{bulk}	bulk ammonia mass fraction (-)
X	Martinelli parameter $=\sqrt{-(dP/dz)_{f,L} / -(dP/dz)_{f,V}}$
X_{tt}	turbulent-turbulent Martinelli parameter
x_{bulk}	bulk ammonia mass fraction
$\tilde{x}$	mole fraction in liquid phase
x	mass fraction in liquid phase
$\tilde{y}$	mole fraction in vapor phase

y	mass fraction in vapor phase
z	ratio of less volatile molar flux to total flux

Greek Symbols

α	heat transfer coefficient (W m^{-2} K^{-1})
α'	apparent heat transfer coefficient (W m^{-2} K^{-1})
β	mass transfer coefficient (m s^{-1}), volumetric quality (-)
δ	liquid film thickness (m)
ε	void fraction (-)
η	efficiency (-)
ρ	density (kg m^{-3})
σ	surface tension (N m^{-1})
Φ	two-phase multiplier (-)
μ	dynamic viscosity (kg m^{-1} s^{-1})
κ	Ackerman [1] correction factor (-)

Subscripts and Superscripts

1	more volatile species in binary mixture (ammonia)
2	less volatile species in binary mixture (water)
a	annular
avg	average
CAT	closest approach temperature
cond	condenser
evap	evaporator
f	friction
HT	heat transfer
HX	heat exchanger
i	segment inlet
int	interface
L	liquid phase
LO	liquid only
LM	logarithmic mean
n-a	non-annular
mix	mixture
o	segment outlet
recup	recuperator
s	isentropic
seg	model segment
sink	thermal sink
source	thermal source
S,V	sensible heat load, vapor
T	total
turb	turbine
V	vapor phase

1. INTRODUCTION AND MOTIVATION

Low-grade (T < 150°C) waste heat remains a vast untapped resource for sustainable production of cooling, heating, or power, with the potential to reduce primary energy consumption in the United States by 12% [2]. It is estimated that ~1.05×10^9 GJ of thermal energy is available per year at temperatures from 100°C to 149°C [2]. Presently, waste heat-to-electricity technology for low and midgrade thermal resources has been primarily limited to Organic Rankine cycles (ORC) and Kalina cycles [3]. These systems use a single (ORC) or multi-component (Kalina) fluid such as propane, butane, R-245fa or ammonia/water mixtures as the working fluid, and are typically deployed for waste heat source temperatures greater than 200°C and large power capacities (> 500 kWe). Furthermore, they are generally custom built for a specific application, resulting in high capital cost (~1100 to 3500 $/kWe) [3].

To fully realize the potential of waste heat for power, smaller (~ 1 to 10 kWe), lower temperature (T_{source} < 150°C) sources must be exploited; these include exhaust gases from coal power plants, gas fired boilers, process steam condensate, cooling water from air-compressors and internal combustion engines, and emissions from other industrial processes. Attaining this goal requires mitigating two key challenges. First, economical recovery of low-grade waste heat is difficult due to thermodynamic (Carnot) limitations. A second, related challenge is that the relativity low thermodynamic efficiencies require that large amounts of heat must be transferred to obtain a useful work output. To maximize efficiency, this heat transfer must occur over as small of a temperature difference as possible, requiring large heat transfer areas and more costly heat exchangers.

One potential pathway for economic distributed generation is to move from custom designed plants to mass-produced, packaged waste heat recovery systems, similar to unitary HVAC

equipment. Development of these systems will require compact, highly effective, heat exchangers, which necessitates accurate methods of predicting heat and mass transfer of the working fluid. Thus, in the present work, we will explore the feasibility of using a microchannel condenser for a 1 kWe Kalina cycle and assess the effect of the different heat and mass transfer models on predicted heat exchanger size, which is directly related to system cost.

2. Prior Work

Kalina cycles have shown potential for efficiently producing power from low temperature thermal resources [4]. This vapor power cycle uses a zeotropic mixture of ammonia and water (and potentially other fluids [5]) as the working fluid. Since zeotropic mixtures are used, the boiling point at a fixed pressure can be altered by changing the bulk fluid composition, allowing for efficient internal recuperation and temperature glide matching to sensible sources during evaporation/condensation. This flexibility has resulted in the proliferation of numerous Kalina configurations [6], each designed to most efficiently operate between a specific temperature source and sink. An example of one such cycle is shown schematically in Fig. 1 (Kalina cycle configuration KCS 34 as defined in [7]), consisting of a turbine, pump, phase separator, and three different heat exchangers. In practice, the Kalina cycle has been successfully deployed as large capacity bottoming cycle and for low-temperature geothermal power generation.

Kalina cycles have been the subject of numerous thermodynamic analysis in the literature [4–6,8–11]. These studies have focused on evaluating different configurations of the cycle with different source and sink temperatures using waste heat/bottoming cycle [4,8,11,12], solar [13–15], geothermal [10,16–18], or other heat sources as an input. After building a thermodynamic state point model of the cycle, optimal operating conditions such as evaporator pressure and bulk ammonia mass fraction can be found [16,19]. Generally, these studies stop at this point and do

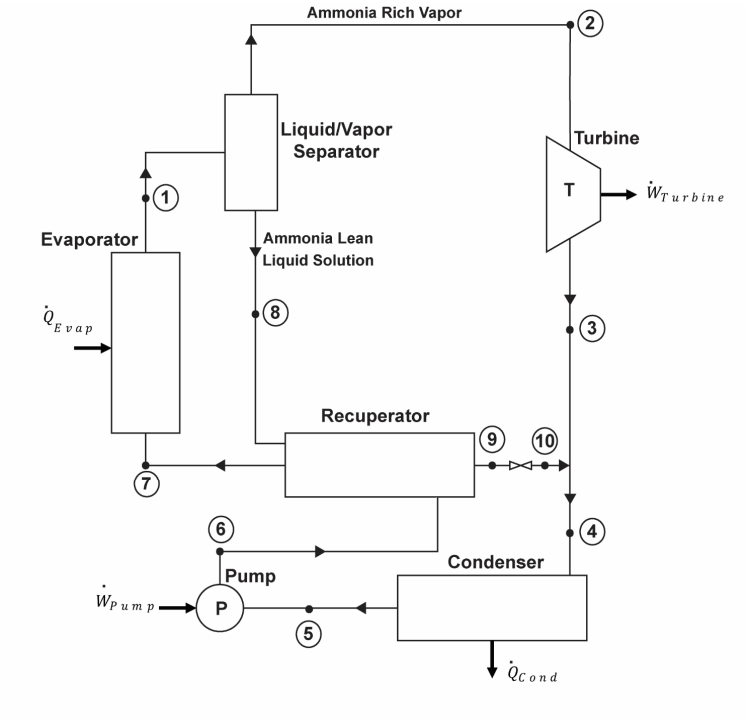

Fig. 1: Kalina cycle schematic

not consider the heat exchanger design and size, which is the key enabling technology for achieving the theoretical performance identified in thermodynamic studies, and a primary source of cost for this cycle [3].

Kim *et al*. [20] noted that assessment of pinch point in an ammonia/water heat exchangers is significantly more difficult than for a pure substance, due to the rapidly changing temperature distribution. In addition, several practical heat exchange design issues impede scaling of the Kalina cycle from large capacity to smaller systems. Due to the corrosive nature of the ammonia/water mixture, stainless or carbon steel heat exchangers must be utilized. This increases cost, size and weight of the system. Furthermore, the toxicity of ammonia has led to resistance in deploying ammonia-based systems in sensitive residential or commercial areas. Microchannel heat exchangers are well suited to overcoming all of these obstacles. By increasing the heat transfer coefficient and surface area-to-volume ratio, the component size can be reduced.

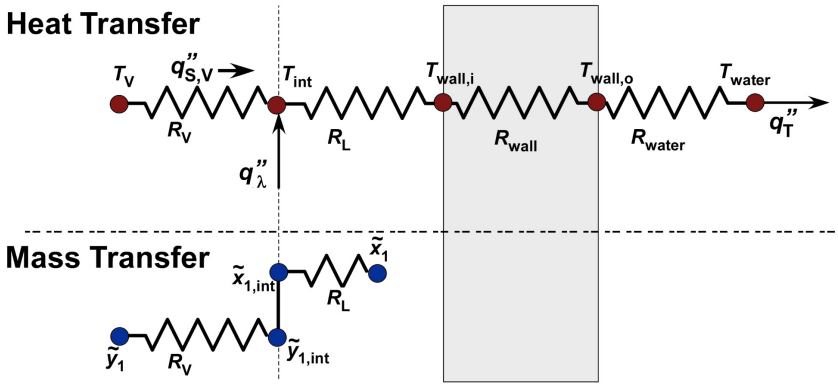

Fig 2. Schematic of coupled heat and mass transfer resistances during zeotropic condensation

This reduction in component size also decreases the working fluid inventory, which may mitigate some safety concerns. Garimella and co-workers [21–23] have successfully demonstrated microchannel technology for similar packaged ammonia/water absorption systems. Design of these microchannel exchangers is dependent on accurately modeling the underlying heat and mass transfer in small diameter channels.

2.1 Zeotropic Heat and Mass Transfer

Unlike the design of evaporators and condensers in standard Rankine or Organic Rankine cycles, zeotropic mixtures exhibit a temperature glide (*i.e.*, difference between dew point and bubble point at a fixed pressure) during phase change due to the changing composition of the vapor and liquid phases. This introduces coupled heat and mass transfer resistances (Fig. 2).

Many experimental studies showed a degradation in heat transfer coefficient during condensation of zeotropic mixtures [24,25]. This means that the measured apparent heat transfer coefficient is lower than the weighted average of the predicted heat transfer coefficients of the individual pure components. Fronk and Garimella [25] found that this degradation was particularly important for high-glide mixtures such as the ammonia/water mixture of interest here. This suggests that applying conventional condensation models that fail to account for the additional mass transfer

resistance when designing Kalina cycle condensers will yield undersized heat exchangers [24,26].

Two common methods for modeling condensation of zeotropic mixtures are the non-equilibrium film method and the equilibrium approach. The non-equilibrium method is based on the work of Colburn and Drew [27], which idealizes the coupled heat and mass transfer resistances as shown previously in Fig. 2. In this approach, thermodynamic equilibrium applies only at the liquid/vapor interface and the transition from the bulk vapor concentration and temperature is assumed to occur through a thin film adjacent to the interface [28]. If appropriate correlations are available for the underlying resistances in Fig. 2, the system of equations can be solved to calculate the heat duty. Investigators [29–31] have applied this modeling framework to many different systems; altering the underlying heat and mass transfer correlations and assumptions (*e.g.*, laminar falling film, annular flow, neglect sensible cooling, etc.) depending on operating conditions.

While more theoretically sound, the non-equilibrium method of condenser design for binary and multi-component mixtures can require substantially more computational resources. Thus, as an alternative modeling approach, the equilibrium or so-called Silver-Bell-Ghaly (SBG) method [32,33] is often used for designing zeotropic condensers, particularly in HVAC&R applications [34]. Here, the vapor-phase mass transfer is not explicitly calculated, but rather accounted for through a mixture resistance correction factor (R_{mix}), as shown in Eq. (1). The mixture resistance correction can then be used to develop an *apparent* condensation heat transfer coefficient, shown in Eq. (2).

$$R_{\text{mix}} = \left(\frac{\dot{Q}_{\text{S,V}}}{\dot{Q}_{\text{T}}} \right) \left(\frac{1}{\alpha_{\text{V}}} \right) \tag{1}$$

$$\alpha_{\mathrm{L}}^{'} = \left[\frac{1}{\alpha_{\mathrm{L}}} + R_{\mathrm{mix}} \right]^{-1} \tag{2}$$

The original justification for Eq. (1) provided by Bell and Ghaly [33] is that calculating the sensible heat transfer coefficient in the vapor phase will result in a significant under prediction of the actual heat transfer, since no two-phase enhancement effects are considered. Thus, the additional resistance from mass transfer that is not calculated is compensated for by underestimating the vapor heat transfer coefficient.

Application of these general modeling techniques remains relatively unexplored in mini and microchannel systems [30,35]. In addition, Deng *et al*. [36] found that predicted condenser length can vary significantly depending on what modeling approach is followed for R134a/R123 systems. The present investigation seeks to better understand how these different models can affect the calculated size of microchannel heat exchangers for Kalina cycle applications. Thus, this paper establishes representative inputs for a microchannel condenser design using a thermodynamic model of the Kalina cycle pictured in Fig. 1. The bottoming condenser (state 4 to 5) of this cycle is then sized using different methods for predicting the ammonia/water heat transfer. The results show the sensitivity of the calculated component size to the assumed model.

3. Kalina System Model

A thermodynamic state point model of a Kalina cycle with a low temperature heat input (150°C) was developed. This model was then used to establish the baseline conditions (e.g., required heat duty, fluid flow rates, inlet temperature/pressure, etc.) for the microchannel condenser design model. The system analyzed is shown schematically in Fig. 1. This Kalina cycle configuration has shown good potential for low temperature power production [6]. The system was coupled to a liquid heat source and sink, operating at 150°C and 20°C, respectively.

Table 1: Assumptions for cycle analysis

Input	Value
$\dot{W}_{net}$	1 kWe
T_{source}	150°C
T_{sink}	20°C
$T_{CAT,evap}$	5 K
$T_{CAT,cond}$	5 K
$T_{CAT,recup}$	4 K
Quality @ State 5	0 (saturated)
η_{turb}	80%
η_{pump}	90%

Starting at state point 1, an ammonia/water multiphase mixture leaves the evaporator at some temperature below the source temperature (*i.e.*, $T_1 = T_{source} - T_{CAT,evap}$) and enters a liquid/vapor separator. At state 2, ammonia rich vapor enters the turbine and expanded to state 3, producing work. At the turbine outlet, the ammonia lean liquid solution that was separated (state 10) is mixed with the ammonia rich turbine outlet, and the combined mixture enters the condenser (state 4). Here, it is completely condensed to a saturated condition before being pumped back to the evaporator pressure (state 6). Finally, energy is recovered in a high temperature recuperator before the mixture is heated through the evaporator back to state 1. Analysis of the cycle required assumptions for closest approach temperature (CAT) in the evaporator, condenser and internal recuperator, and efficiency of the pump and turbine, as summarized in Table 1. Pressure drop through the heat exchangers and separator was neglected.

A summary of equations used to analyze each component is provided in Table 2. For each state point, relations were developed for three independent, intensive thermodynamic properties, which then fixed the remaining thermodynamic properties at that point. Energy and mass balances provided closure to the thermodynamic model. Thermodynamic property data of the ammonia/water mixture was calculated using NIST REFPROP 9.0 [37]. Using the developed model, total mass flow rate required to achieve 1 kWe net power output and the cycle thermal

Table 2: Kalina cycle thermodynamic model state points model relations

State		Equation
1	Evaporator Outlet	$T_1 = T_{\text{source}} - T_{\text{CAT,evap}}$ $P_1 = P_{\text{high}}$ $x_{\text{bulk},1} = x_{\text{bulk}}$
2	Vapor Separator Outlet/Turbine Inlet	$T_2 = T_1$ $P_2 = P_1$ $x_{\text{bulk},2} = x_{\text{v},1}$
3	Turbine Outlet	$P_3 = P_5$ $x_{\text{bulk},3} = x_{\text{bulk},2}$ $\eta_{\text{turb}} = \frac{h_2 - h_3}{h_2 - h_{3,s}}$
4	Condenser Inlet	$P_4 = P_5$ $x_{\text{bulk},4} = x_{\text{bulk}}$ $h_4 = q_1 \cdot h_3 + (1 - q_1) h_{10}$
5	Condenser Outlet	$T_5 = T_{\text{sink}} + T_{\text{CAT,cond}}$ $q_5 = 0$ $x_{\text{bulk},5} = x_{\text{bulk}}$
6	Pump Outlet/Recuperator Low Temperature Inlet	$P_6 = P_1$ $x_{\text{bulk},6} = x_{\text{bulk},1}$ $\eta_{\text{pump}} = \frac{h_5 - h_{6,s}}{h_5 - h_6}$
7	Recuperator Low Temperature Outlet/Evaporator Inlet	$P_7 = P_1$ $x_{\text{bulk},7} = x_{\text{bulk},1}$ $\dot{m}_{lean}(h_8 - h_9) = \dot{m}(h_7 - h_6)$
8	Liquid Separator Outlet/Recuperator High Temperature Inlet	$T_8 = T_1$ $P_8 = P_1$ $x_{\text{bulk},8} = x_{\text{v},1}$
9	Recuperator High Temperature Outlet	$T_9 = T_7 + T_{\text{CAT,recup}}$ $P_9 = P_1$ $x_{\text{bulk},9} = x_{\text{bulk},8}$
10	Expansion valve outlet	$P_{10} = P_5$ $x_{\text{bulk},10} = x_{\text{bulk},9}$ $h_{10} = h_9$
-	Cycle Net Work	$\dot{W}_{net} = \dot{W}_{turb} + \dot{W}_{pump} = 1\ \text{kW}$ $\dot{W}_{net} = \dot{m}_{rich}(h_2 - h_3) + \dot{m}(h_5 - h_6)$
-	Condenser Heat Duty	$\dot{Q}_{cond} = \dot{m}(h_5 - h_4)$

efficiency were calculated at varying bulk ammonia mass fraction (x_{bulk}) and evaporator pressure,

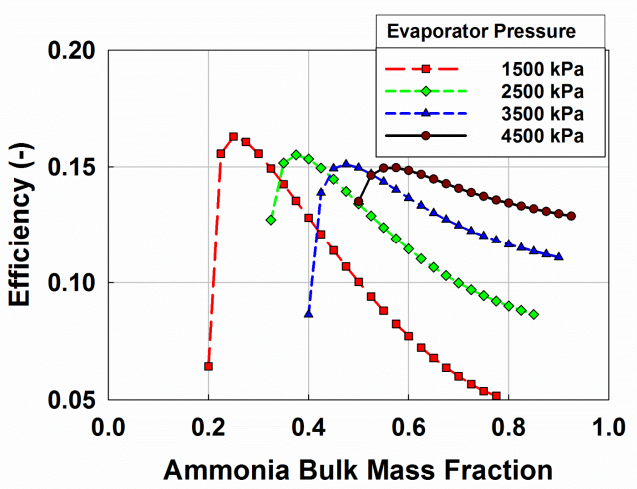

Fig 3. Kalina cycle simulated efficiency versus bulk ammonia mass fraction at different evaporator pressures

with the results summarized in Fig. 3.

Fig. 3 shows that for a constant pressure, the thermal efficiency initially increases with bulk ammonia mass fraction, reaches a maximum and then decreases. These results are consistent with other Kalina cycle models from the literature [5]. Investigators have determined different optimal bulk ammonia mass fraction depending on the source temperature of interest, ranging from 50 to 90% [6]. Qualitative evaluation of Fig. 3 shows that for leaner ammonia mass fraction (below the maximum efficiency point), the drop off in efficiency is drastic. Thus, for stable operation it is desirable to operate away from this point, to allow for better performance for varying evaporation pressure.

In the present study, a bulk ammonia mass fraction of 0.5 and evaporation pressure of 3500 kPa were chosen. The calculated overall efficiency was 14.9%, using the assumptions in Table 1. These conditions yielded an overall mass flow rate of 0.0163 kg s^{-1} for the ammonia/water mixture through the condenser, assuming 1 kWe of net power generation. In addition, the condenser inlet conditions were at a temperature of 43.7°C, pressure of 322 kPa, and quality of 0.18. Interestingly,

Table 3: Microchannel heat exchanger model inputs

Input	Value
$\dot{Q}_{cond}$	5.7 kW
Working fluid-side	
$\dot{m}_{NH_3/H_2O}$	0.0163 kg/s
$P_{NH3/H2O,in}$	322 kPa
x_{bulk}	0.5
$T_{NH3/H2O,in}$	43.7°C
$T_{NH3/H2O,out}$	25.0°C
Δq	0.18
ΔP_{max}	11 kPa
Water-side	
$\dot{m}_{water}$	0.25 kg/s
$T_{water,in}$	20°C

the condenser is only required to partially condense the fluid, yielding a total required condenser heat duty of 5.7 kW. The thermodynamic quality is reduced at the condenser inlet when the ammonia lean solution (state 10) is mixed with the ammonia rich solution (state 3) from the turbine outlet.

4. Ammonia/Water Microchannel Heat Exchanger Model

The results from the baseline system model were used as inputs (Table 3) for determining the required condenser area using different microchannel heat exchanger models. The total required condenser heat duty was 5.7 kW. The total cooling water flow rate was specified to yield a 5 K temperature increase. Notably, the NH_3/H_2O mixture undergoes a temperature change of 18.7 K, suggesting that an account of significant coupled heat and mass transfer effects is required.

4.1 Heat Exchanger Geometry and Modeling Approach

The condenser was modeled as a slab consisting of two adjacent sets of parallel circular microchannels (shown in Fig. 4a, without a headering system). Headers (not shown), would distribute the water and working fluid to either the top or bottom array of parallel microchannels, where the two fluids are oriented for counterflow. The length of the heat exchanger was defined as the flow length of the channels, while the width was equal to the number of channels plus the

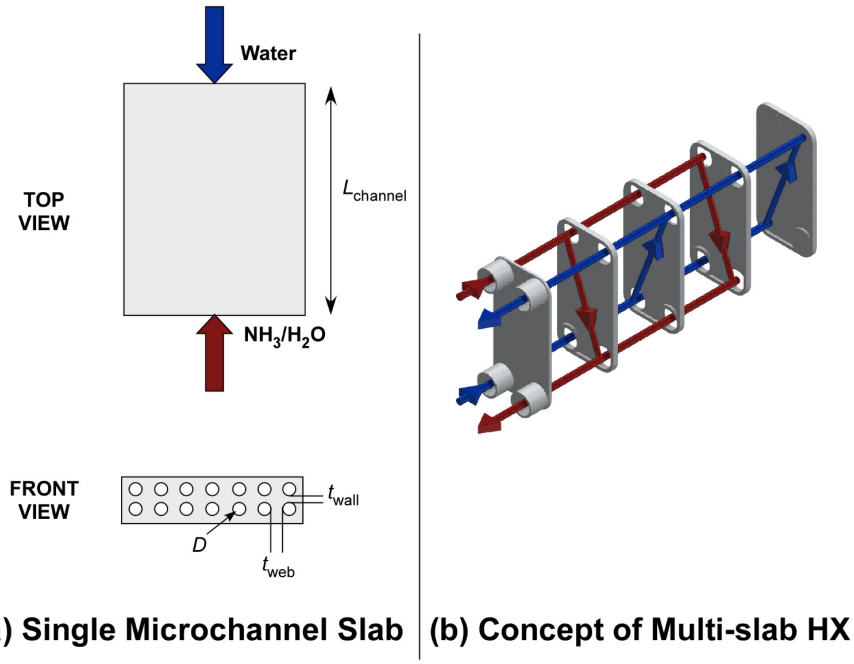

Fig 4. Schematic of (a) single microchannel heat exchanger slab and (b) concept of multi-slab microchannel heat exchanger

web thickness between each channel. It was assumed that the heat exchanger was constructed of carbon steel. For the present analysis, D = 0.5 mm, t_{web} and t_{wall} = 2 mm. The number of channels was varied to maintain the predicted pressure drop below the maximum allowable pressure drop, discussed in Section 5.

While likely not practical as an actual heat exchanger design, the modeled geometry allows easy visualization of the effect of the change in predicted heat transfer area due to different microchannel heat and mass transfer modeling approaches. In an actual microchannel heat exchanger, this slab could be divided into multiple shims of equal size and manufactured into a single plate type heat exchanger (concept shown in Fig. 4b), such as those experimentally demonstrated for ammonia/water absorption heat pumps by Garimella and co-workers [21,22].

To account for the varying thermodynamic properties, phase compositions and temperatures, a nodal analysis was developed using the *Engineering Equation Solver (EES)* platform [38],

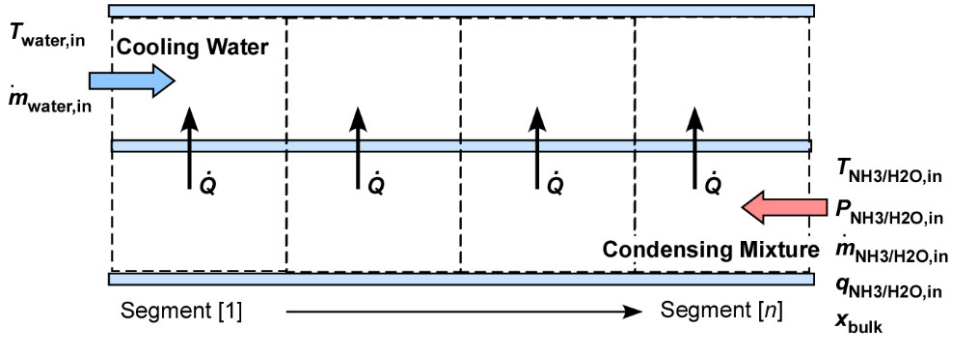

Fig. 5: Schematic of segmented model

shown schematically in Fig. 5. The heat exchanger was divided into constant length segments of L_{seg} = 7.5 mm. Each segment was modeled as a counterflow heat exchanger. In each segment the water thermal resistance (R_{water}) was calculated using the single-phase Churchill [39] correlation, valid for laminar, transition and turbulent flow. For the geometries considered, the water remained laminar, with $650 < Re_w < 704$. The wall thermal resistance (R_{wall}) was calculated considering the wall thickness (2 mm) between the water and working fluid channels, and a constant thermal conductivity (k = 50 W m^{-1} K^{-1}) for carbon steel (required for compatibility with NH_3/H_2O). For each segment, the heat transfer in the ammonia/water mixtures and the segment heat duty were calculated using either different versions of the equilibrium or non-equilibrium model, detailed below.

4.2 Ammonia/Water Heat Transfer Resistance

Non-Equilibrium Model

Based on the non-equilibrium framework of Colburn and Drew [27], Fronk and Garimella introduced [40] and experimentally verified a non-equilibrium model for high-glide, binary zeotropic mixtures of NH_3/H_2O in microchannels. This framework was used to predict the heat transfer in the present study. The coupled heat and mass transfer resistance in the microchannel were modeled according to the resistance diagram shown previously in Fig 2. Expressions for each

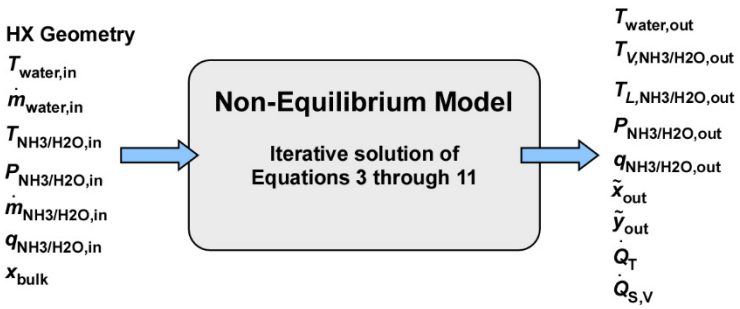

Fig. 6: Non-equilibrium model inputs and outputs

resistance are described below. Then, a system of equations is solved iteratively for given set of inputs to provide the key outputs of heat transfer rate per segment (Fig. 6). A more detailed description of the framework and investigation of the verification of the underlying assumptions can be found in Refs. [30,40].

In each segment, the vapor-phase sensible heat transfer was determined from Eq. (3), where the vapor-phase heat transfer coefficient was determined from Ref. [39]. The correction factor κ (Eq. (4)), accounts for the effect of the condensing flux on the sensible heat transfer [1], while the vapor-phase log mean temperature (Eq. (5)) accounts for the driving temperature difference from the vapor bulk to the liquid/vapor interface.

$$\dot{Q}_{S,V} = \alpha_V \cdot \kappa \cdot \left(\pi \cdot D \cdot L_{seg}\right) \cdot \Delta T_{LM,V} \tag{3}$$

$$\kappa = \frac{a}{1-\exp\left(-a\right)} \tag{4}$$

where

$$a = \frac{m'' \cdot c_{P,V}}{\alpha_V}$$

$$\Delta T_{LM,V} = \frac{\left(T_{v,i} - T_{int,i}\right) - \left(T_{v,o} - T_{int,o}\right)}{\ln\left(\dfrac{T_{v,i} - T_{int,i}}{T_{v,o} - T_{int,o}}\right)} \tag{5}$$

The condensing ammonia ($\dot{N}_1$) and water ($\dot{N}_2$) molar rates are determined from Eq. (6). Here, the vapor phase mass transfer coefficient (β_V) is determined via the Chilton-Colburn [41] analogy, and z is defined as $\dot{N}_1/\dot{N}_T$. The interfacial mole fraction of ammonia ($\tilde{y}_{1,\text{int,avg}}$) is calculated from the average interface temperature ($T_{\text{int,avg}}$), assuming thermodynamic equilibrium and a well mixed liquid film (i.e., liquid film interface mole fraction is equal to the bulk liquid interface mole fraction). It should be noted that the calculation of $T_{\text{int,avg}}$ is an iterative process.

$$\dot{N}_1 + \dot{N}_2 = \dot{N}_T = \beta_V \cdot C_V \cdot \ln\left(\frac{z - \tilde{y}_{1,\text{int,avg}}}{z - \tilde{y}_{1,\text{avg}}}\right) \tag{6}$$

With expressions for the vapor sensible heat and condensing flux developed, the total heat transfer from the working fluid to the water can be modeled by Eq. (7), where R_{wall} and R_{water} were calculated as described above (Section 4.1).

$$\dot{Q}_T = \frac{\Delta T_{\text{LM,int}}}{R_L + R_{\text{wall}} + R_{\text{water}}} \tag{7}$$

Finally, mass (Eq. (8)), species (Eq. (9)), and energy (Eq. (10)) balances for each phase are applied, and the interfacial temperatures and interfacial vapor/liquid concentrations were found by enforcing the thermodynamic equilibrium condition at the interface. This provided closure to the set of equations, and allowed the segment heat duty to be found. The outlet phase temperatures and compositions were used as inlet conditions for the subsequent constant length segments. The model repeated until a saturated liquid outlet was achieved. The total required channel length could then be determined, which fixes the required heat exchanger size.

Mass balance:

$$\begin{aligned} \dot{m}_{\mathrm{L,O}} &= \underbrace{\dot{m}_{\mathrm{L,i}}}_{\text{Mass flow liquid in}} + \underbrace{m_1^{''} \cdot A}_{\text{Mass Flow } NH_3 \text{ condensed in}} + \underbrace{m_2^{''} \cdot A}_{\text{Mass Flow } H_2O \text{ condensed in}} \\ \dot{m}_{\mathrm{V,O}} &= \underbrace{\dot{m}_{\mathrm{V,i}}}_{\text{Mass flow vapor in}} - \underbrace{m_1^{''} \cdot A}_{\text{Mass Flow } NH_3 \text{ condensed in}} - \underbrace{m_2^{''} \cdot A}_{\text{Mass Flow } H_2O \text{ condensed in}} \end{aligned} \tag{8}$$

Species balance:

$$\begin{aligned} x_{\mathrm{l,O}}\dot{m}_{\mathrm{L,O}} &= \underbrace{x_{\mathrm{l,i}} \cdot \dot{m}_{\mathrm{L,i}}}_{\text{Mass Flow } NH_3 \text{ in}} + \underbrace{m_1^{''} \cdot A}_{\text{Mass Flow } NH_3 \text{ condensed in}} \\ y_{\mathrm{l,O}}\dot{m}_{\mathrm{V,O}} &= \underbrace{y_{\mathrm{l,i}} \cdot \dot{m}_{\mathrm{V,i}}}_{\text{Mass Flow } NH_3 \text{ in}} - \underbrace{m_1^{''} \cdot A}_{\text{Mass Flow } NH_3 \text{ condensed out}} \end{aligned} \tag{9}$$

Energy balance:

$$\begin{aligned} \dot{m} \cdot h_{\mathrm{o,T}} &= \dot{m}_{\mathrm{V,O}} h_{\mathrm{V,O}} + \dot{m}_{\mathrm{L,O}} h_{\mathrm{L,O}} \\ h_{\mathrm{o,T}} &= h_{\mathrm{i,T}} - \frac{\dot{Q}_T}{\dot{m}} \end{aligned} \tag{10}$$

Fronk and Garimella [40] showed that liquid film heat transfer coefficient (α_L) correlation used to calculate the liquid thermal resistance (R_L, Eq. (11)) was the most important input to the above non-equilibrium film model approach for ammonia/water mixtures in small channels. They found that liquid-phase condensation correlations [42–45] developed for fluid with significantly different properties or in larger channels than the ammonia/water mixtures exhibited poorer agreement with the data when used in the film model.

$$R_L = \frac{1}{\alpha_{\mathrm{L}} A_{\mathrm{HT}}} \tag{11}$$

Thus, to assess the effect of the liquid-phase condensation heat transfer coefficient on Kalina cycle condenser size, two different microchannel condensation models were considered within the non-equilibrium framework described here. The first was a correlation developed [40] for pure ammonia in small channels ($0.98 < D < 2.16$ mm) and at low mass fluxes ($50 < G < 225$ kg m^{-2} s^{-1}). The second was the comprehensive mini/microchannel correlation of Kim and Mudawar [45], which was developed from a large database of 17 different working fluids,

hydraulic diameters from 0.424 to 6.22 mm, mass flux from 53 to 1403 kg m^{-2} s^{-1}, and reduced pressure from 0.04 to 0.91. Description of both models are provided in Appendix A.

Equilibrium Film Model

The second category of model considered was the equilibrium approach, described in Section 2. In the present work, α_V in Eq. (1) was calculated from [39], while α_L in Eq. (2) was calculated using either the ammonia correlation of Fronk and Garimella [40], the comprehensive mini/microchannel correlation of Kim and Mudawar [45], or the macrochannel condensation correlation of Shah [44] (provided in Appendix A). A comparison of these results is provided in the following section.

Once the apparent liquid film heat transfer coefficient (Eq. (2)) was known, the segment heat duty could be determined based on the heat transfer area, and wall and water-side thermal resistances, calculated as above. The process was repeated for subsequent segments until the required channel length for complete condensation was determined.

5. Condenser Design Results Using Different Heat and Mass Transfer Models

5.1 Design Procedure

In the present analysis, the channel diameter, wall and web thickness, total heat duty, total working fluid and water mass flow rate were initially fixed according to the geometry in Section 4.1 and the heat exchanger operating conditions in Table 3. The free geometric variables in the microchannel heat exchanger design were the channel length and number of parallel channels, and it was assumed that the water and working fluid were uniformly distributed between the parallel channels.

While microchannels offer very high heat transfer coefficients, they also tend to result in large frictional pressure gradients, which are detrimental to overall system efficiency. In the present analysis, a maximum allowable pressure drop of 11 kPa was enforced. This pressure loss corresponds to a 1 K saturation temperature loss at the saturated liquid state for the given pressure and bulk ammonia concentration. Since the closest approach temperature between the saturated liquid outlet and the incoming cooling water is only 5 K, any greater pressure loss would significantly reduce the driving temperature difference and the related heat transfer.

Starting with an assumption of 900 parallel channels, the length of each channel was determined from the above analysis, and the two-phase microchannel pressure drop was determined using the correlation of Keinath [46]. This model uses the microchannel void fraction model of Keinath and Garimella [47] for closure, and was verified and developed for channel sizes similar to those in the present analysis. Both of these models are presented in Appendix A.

If the pressure drop was greater than 11 kPa, the number of parallel channels was increased in 25 channel increments until the calculated pressure drop was less than the threshold and the heat duty requirement was satisfied. The pressure drop is primarily a function of the channel length and the fluid mass flux. As the number of channels increases, the mass flux per channel decreases, which tends to decrease pressure drop. However, this also decreases the heat transfer coefficient, which can lead to a longer heat exchanger to achieve the desired heat duty. By carefully considering these coupled effects, a realistic heat exchanger design was developed. For the all of the modeling approaches, heat exchanger lengths varied from 12.75 to 18.8 cm and from 1025 to 1100 parallel channels to maintain the pressure drop below 11 kPa.

5.2 Discussion of Results

The outputs of the above analysis using the five different heat transfer modeling approaches (two non-equilibrium models using correlations of [40,45], and three equilibrium model using

Table 4: Calculated heat exchanger parameters for each microchannel modeling approach

	$N_{channel}$	$L_{channel}$	G (kg m^{-2} s^{-1})
Non-Equilibrium Models:			
Fronk and Garimella [40]	1025	12.75 cm	81.1
Kim and Mudawar [45]	1075	14.25 cm	77.4
Equilibrium Models:			
Fronk and Garimella [40]	1025	15.00 cm	81.1
Kim and Mudawar [45]	1100	16.40 cm	75.6
Shah [44]	1100	18.80 cm	75.6

correlations of [40,44,45]) while maintaining a maximum pressure drop were (a) Number of parallel channels (b) Channel length, and (c) Mass flux per channel, shown in Table 4. The channel length and number of channels were then used to determine the total heat exchanger slab area (calculated via Eq. (12)) with the results for each approach shown in Fig. 7.

$$A_{HX} = N_{channel} \times \left(D + t_{web} \right) \times L_{channel} \tag{12}$$

Figure 7 shows that the non-equilibrium model using the Fronk and Garimella correlation produced the smallest overall heat exchanger. The equilibrium models yielded designs 18, 38 and 58% larger using the Fronk and Garimella [40], Kim and Mudawar [45] and Shah [44] models,

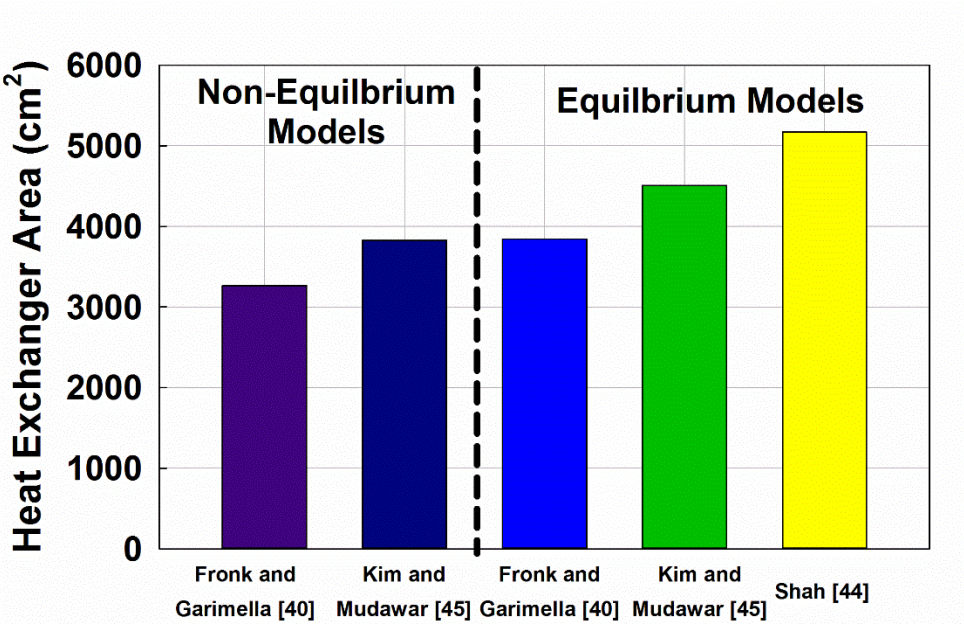

Fig. 7: Heat exchanger area versus condensation modeling approach

respectively. Furthermore, the non-equilibrium models using the Fronk and Garimella [40] and Kim and Mudawar [45] liquid film correlations yielded smaller heat exchanger areas compared to the equilibrium approach using the same correlations (15% smaller for Fronk and Garimella [40] and 15% smaller for Kim and Mudawar [45]). These results can be attributed to the large condensation temperature glide of these mixtures, which result in artificially large apparent mixtures resistance (Eq. (1)), degrading the apparent heat transfer coefficient and increasing the required heat transfer area. To illustrate this, Figure 8a shows the calculated "uncorrected" condensation heat transfer coefficient using the Fronk and Garimella [40] correlation compared with the "corrected" apparent heat transfer coefficient (Eq. (2)) along the condenser length for the same equilibrium conditions. Near the condenser inlet, where the temperature glide is largest, there is a significant degradation in predicted heat transfer coefficient due to the mixture resistance

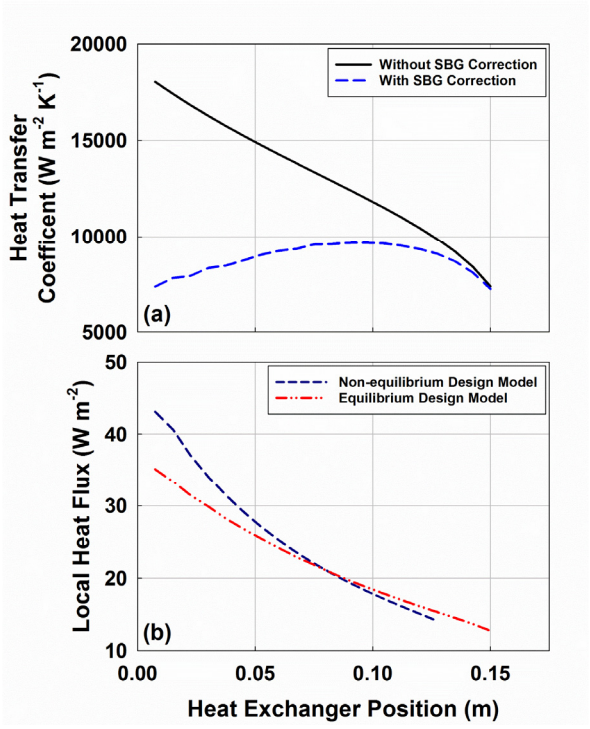

Fig. 8: Comparison of (a) Fronk and Garimella [40] heat transfer coefficient with and without Silver-Bell-Ghaly correction factor and (b) local heat flux of non- equilibrium and equilibrium condenser design model

correction factor (Eq. (1)), which is intended to account for mass transfer resistance. Towards the end of the condenser where only ammonia vapor remains and the local temperature glide approaches zero, the heat transfer coefficients converge (i.e, the mixture resistance correction → 0). However, consider Figure 8b, which shows a comparison of predicted local heat flux along the condenser for the equilibrium and non-equilibrium approaches using the Fronk and Garimella [40] correlation. The non-equilibrium model, which explicitly accounts for mass transfer, shows higher heat fluxes than the equilibrium model towards the condenser inlet, suggesting the lumped approach of the equilibrium model may be overpredicting the mass transfer effects resistances of these mixtures. Because of this, the non-equilibrium condenser is predicted to be smaller for the same heat duty. Near the outlet of both condensers, the predicted heat fluxes of each model approach one another, as the mass transfer effect diminish.

While more computationally intensive, the non-equilibrium approach was shown previously [25,40] to provide better predictive capability of experimental data than the equilibrium models for NH_3/H_2O mixtures in a single tube. These results were also consistent with the findings of Deng *et al*. [36], who found that a non-equilibrium modeling approach provided a better prediction than equilibrium models for predicting the experimental condensation length required for a mixture of R134a/R23 (0.349/0.651 by mass).

If the goal of using microchannel heat exchangers is to decrease component size and cost as much as possible, the results suggest that the more computationally intensive non-equilibrium model, in which the coupled effects of heat and mass transfer are accounted for will provide a more compact design. It should be noted that the present analysis was conducted for a water-coupled condenser, in which the ratio of the working fluid resistance to the water-side resistance was nearly unity ($R_{ratio,avg}$ = 0.9, $R_{ratio,max}$ = 2.14, $R_{ratio,min}$ = 0.45). For air-coupled condensers,

where the air-side resistance is expected to be much greater, the required heat transfer area may be less sensitive to the selected working fluid heat transfer model.

Another interesting observation are that the maximum mass fluxes allowed by the pressure drop constraint are relatively low ($G < 81.1$ kg m^{-2} s^{-1}) and that the specified heat exchangers have high aspect ratio (short flow length versus a large face area) and thousands of multiple channels. Much of the experimental work on single and multi-component condensation in small channels has been conducted at higher mass fluxes [26]. These prior studies have shown a strong effect of mass flux on heat and mass transfer in mini and microchannels. Thus, many of the empirical and semi-empirical models that have been developed from relatively high-flux laboratory experiments may not be applicable for the design of actual heat transfer equipment.

6. Conclusions

The results presented here demonstrate the effect of different heat and mass transfer models on the size of heat exchangers required to enable small-scale ammonia/water Kalina power systems. As shown, these systems can efficiently (14.9% for the baseline conditions here) generate electricity using low-grade thermal resources. The basic system analysis presented here is by no means comprehensive. Certainly, there are numerous different Kalina cycle configurations, source/sink temperatures and other assumptions (*i.e.*, closest approach temperature, rotating equipment efficiency, etc.) that can yield different overall efficiency and individual heat exchanger required heat duties. However, the purpose of the baseline cycle analysis was to provide reasonable input variables to the microchannel heat exchanger model for application in a small scale waste heat recovery system. In the system configuration analyzed here, three different heat exchangers are required. In each heat exchanger, zeotropic mixtures of ammonia/water undergo either

evaporation, condensation, or desorption/absorption. All of these processes require careful consideration of the multiphase, coupled heat and mass transfer process.

To assess the sensitivity of component and thus system size to these predictions, the partial condenser was analyzed in detail. A parametric analysis revealed that the non-equilibrium model of Fronk and Garimella [40] produced the smallest heat exchanger, with the equilibrium approaches producing heat exchangers up to 58% larger. In an earlier work, the Fronk and Garimella [40] model showed good agreement with ammonia/water condensation data in a single microchannel tube ($0.98 < D < 2.16$ mm), similar to the conditions in the present study. However, further validation of the approach when scaled to a full condenser is required.

The results for all five heat transfer modeling approaches reveal that hundreds of parallel channels are required to maintain satisfactory pressure drop, resulting in heat exchangers that are nearly as wide as they are long. Furthermore, the results show that the maximum allowable working fluid mass flux was between 75 and 81 kg m^{-2} s^{-1}. For scenarios which require even greater heat duty (*e.g*, 100% condensation versus the approximately 20% in the present analysis), the maximum allowable mass fluxes may be even lower. These results suggest that additional work is required in the following areas:

- Detailed understanding of microchannel flow distribution and header design. These insights will be critical for the adoption of microchannel heat exchangers into compact, kilowatt/megawatt scale heating, cooling, and power systems.
- Understand multiphase microchannel transport phenomena at very low mass fluxes to replicate the conditions that are expected in a real system. This may require the

development of new techniques for dealing with the experimental difficulties of very low flow rates, heat duties and temperature differences.

- Verification of non-equilibrium film model for a full condenser design.
- Understand multiphase, multicomponent heat and mass transfer in micro-geometries other than multiple parallel microchannels to minimize pressure drop while maintaining high heat transfer coefficients. Examples include pin fin arrays or the use of varying diameter fractal like microchannel features [48,49]. These may yield more compact heat exchanger requiring less complicated headering structures.

By designing optimized small-scale systems to exploit vast waste heat resources, nearly carbon neutral capacity can be added without the costly construction of new renewable or non-renewable plants.

APPENDIX A

A.1 Fronk and Garimella [40] Condensation Heat Transfer Model

Determine flow regime:

$$\begin{aligned} &\text{Annular flow} && j_G^* > 2.5 \\ &\text{Non-annular flow} && j_G^* \le 2.5 \end{aligned} \tag{13}$$

where

$$j_{\mathrm{G}}^* = \frac{G \cdot q}{\sqrt{D \cdot g \cdot \rho_{\mathrm{V}} \cdot \left(\rho_{\mathrm{L}} - \rho_{\mathrm{V}}\right)}}$$

For annular flow:

$$\mathrm{Nu}_{\mathrm{a}} = \frac{\alpha D}{k_{\mathrm{L}}} = 0.023 \cdot \mathrm{Re}_{\mathrm{LO}}^{0.8} \cdot \mathrm{Pr}_{\mathrm{L}}^{0.4} \cdot \left(1 + 0.27 \left(\frac{U_{\mathrm{V}}}{U_{\mathrm{L}}}\right)^{0.21} f_{\mathrm{int}}^{-0.46}\right) \tag{14}$$

where

$$f_{\mathrm{int}} = \frac{\left(\rho_{\mathrm{L}} - \rho_{\mathrm{V}}\right) \cdot g \cdot \delta^2}{\sigma}$$

Phase velocities (U_{V} and U_{L}) and film thickness are determined from Keinath and Garimella [47] microchannel condensation void fraction model:

$$\varepsilon = \frac{\beta}{1 + \bar{V}_{\mathrm{vj}} / j} \tag{15}$$

where

$$\bar{V}_{\mathrm{vj}} = 0.336 \cdot X^{0.25} \cdot \mathrm{Ca}_{\mathrm{L}}^{0.154} \left(\sqrt{\frac{\rho_{\mathrm{L}}}{\rho_{\mathrm{V}}}} - 1\right)^{0.81} j$$

For non-annular flow:

$$\mathrm{Nu}_{\mathrm{n\text{-}a}} = \frac{\alpha_{\mathrm{L}} D}{k_{\mathrm{L}}} = \left[\mathrm{Nu}_{\mathrm{a}} \left(\frac{2.5}{j_{\mathrm{G}}^*}\right)^{0.8} - \mathrm{Nu}_{\mathrm{wavy}}\right] \left(\frac{j_{\mathrm{G}}^*}{2.5}\right) + \mathrm{Nu}_{\mathrm{wavy}} \tag{16}$$

where

$$\mathrm{Nu}_{\mathrm{wavy}} = \left[\left(1 + 0.741 \left[\frac{1-q}{q} \right]^{0.3321} \right)^{-1} \mathrm{Nu}_{\mathrm{film}} + \mathrm{Nu}_{\mathrm{pool}} \right]$$

$$\mathrm{Nu}_{\mathrm{film}} = \left(\frac{D}{k_{\mathrm{L}}} \right) 0.725 \left(\frac{k_{\mathrm{L}}^3 \rho_{\mathrm{L}} \left(\rho_{\mathrm{L}} - \rho_{\mathrm{V}} \right) g h_{\mathrm{fg}}}{\mu_{\mathrm{L}} D \left(T_{\mathrm{sat}} - T_{\mathrm{wall}} \right)} \right)^{0.25} \tag{17}$$

$$\mathrm{Nu}_{\mathrm{pool}} = 0.023 \, \mathrm{Re}_{\mathrm{LO}}^{0.8} \, \mathrm{Pr}_{\mathrm{L}}^{0.4} \left(1 - q^{0.087} \right)$$

A.2 Kim and Mudawar [45] Condensation Heat Transfer Model

Determine flow regime:

Annular flow $\quad We^* > 7 \cdot X_{tt}^{0.2}$

Non-annular flow $\quad We^* \le 7 \cdot X_{tt}^{0.2}$

where

$$We^* = \frac{2.45 \cdot \mathrm{Re}_{\mathrm{V}}^{0.64}}{\mathrm{Su}_{\mathrm{VO}}^{0.3} \cdot \left(1 + 1.09 \cdot X_{tt}^{0.039} \right)^{0.4}} \quad \text{for} \quad \mathrm{Re}_L \le 1250 \tag{18}$$

$$We^* = \frac{\mathrm{Re}_{\mathrm{V}}^{0.64} \cdot X_{tt}^{0.157}}{\mathrm{Su}_{\mathrm{VO}}^{0.3} \cdot \left(1 + 1.09 \cdot X_{tt}^{0.039} \right)^{0.4}} \cdot \left[\left(\frac{\mu_V}{\mu_L} \right)^2 \cdot \left(\frac{\rho_L}{\rho_V} \right) \right] \quad \text{for} \quad \mathrm{Re}_L > 1250$$

For annular flow:

$$\mathrm{Nu}_{\mathrm{a}} = \frac{\alpha_{\mathrm{L}} D}{k_{\mathrm{L}}} = 0.048 \, \mathrm{Re}_{\mathrm{L}}^{0.69} \, \mathrm{Pr}_{\mathrm{L}}^{0.34} \, \frac{\Phi_{\mathrm{V}}}{X_{\mathrm{tt}}} \tag{19}$$

Where the two-phase multiplier is calculated from Table A.1 [50].

Table A.1 Calculation of two-phase multiplier from Kim and Mudawar [50]

$\Phi_V = \sqrt{1 + C \cdot X + X^2}$		
Re_L	**Re_V**	***C***
Laminar	Laminar	$C = 3\times10^{-5}\,\mathrm{Re}_{LO}^{0.44}\,\mathrm{Su}_{VO}^{0.50}\left(\frac{\rho_L}{\rho_V}\right)^{0.48}$
Laminar	Turbulent	$C = 0.0015\,\mathrm{Re}_{LO}^{0.59}\,\mathrm{Su}_{VO}^{0.19}\left(\frac{\rho_L}{\rho_V}\right)^{0.36}$
Turbulent	Laminar	$C = 8.7\times10^{-4}\,\mathrm{Re}_{LO}^{0.17}\,\mathrm{Su}_{VO}^{0.50}\left(\frac{\rho_L}{\rho_V}\right)^{0.14}$
Turbulent	Turbulent	$C = 0.39\,\mathrm{Re}_{LO}^{0.03}\,\mathrm{Su}_{VO}^{0.10}\left(\frac{\rho_L}{\rho_V}\right)^{0.35}$

For non-annular flow:

$$\mathrm{Nu}_{na} = \left[\left(\mathrm{Nu}_a\right)^2 + \left(3.2\times10^{-7}\,\mathrm{Re}_L^{-0.38}\,\mathrm{Su}_{VO}^{1.39}\right)^2\right]^{1/2} \tag{20}$$

A.3 Shah [44] Condensation Heat Transfer Correlation

$$\mathrm{Nu} = \frac{\alpha_L D}{k_L} = 0.023\,\mathrm{Re}_{LO}^{0.8}\,\mathrm{Pr}_L^{0.4}\cdot\left[\left(1-q\right)^{0.8} + \frac{3.8\cdot x^{0.76}\cdot\left(1-q\right)^{0.04}}{P_r^{0.38}}\right] \tag{21}$$

A.4 Keinath [46] Condensation Pressure Drop Model

$$\left(\frac{dP}{dz}\right) = \frac{0.5\cdot f_K\cdot\rho_V\cdot j_V^2}{D\cdot\varepsilon^{2.5}}$$

where (22)

$$f_K = 0.0007\cdot f_L\cdot X^{0.48}\cdot\mathrm{Re}_{L,\varepsilon}^{0.91}\cdot\left(\frac{Ca_L}{1-\varepsilon}\right)^{-0.258}\cdot\left(\frac{\rho_L}{\rho_V}\right)^{0.1}$$

References

[1] Ackermann, G., 1937, "Heat Transfer and Molecular Mass Transfer in the Same Field at High Temperatures and Large Partial Pressure Differences," VDI-Forschungsheft, **8**(382), pp. 1–10.

[2] Rattner, A. S., and Garimella, S., 2011, "Energy harvesting, reuse and upgrade to reduce primary energy usage in the USA," Energy, **36**(10), pp. 6172–6183.

[3] BCS Incorporated, 2008, Waste Heat Recovery: Technology and Opportunities in U.S. Industry.

[4] Kalina, A. I., 1984, "Combined-Cycle System with Novel Bottoming Cycle," J. Eng. Gas Turbines Power.

[5] Elsayed, A., Embaye, M., AL-Dadah, R., Mahmoud, S., and Rezk, A., 2013, "Thermodynamic performance of Kalina cycle system 11 (KCS11): feasibility of using alternative zeotropic mixtures," Int. J. Low-Carbon Technol., **8**(suppl 1), pp. i69–i78.

[6] Zhang, X., He, M., and Zhang, Y., 2012, "A review of research on the Kalina cycle," Renew. Sustain. Energy Rev., **16**(7), pp. 5309–5318.

[7] Micak, Henry, A., 2002, "Kalina Cycle Concepts for Low Temperature Geothermal," Geothermal Resources Council Transactions.

[8] Bombarda, P., Invernizzi, C. M., and Pietra, C., 2010, "Heat recovery from Diesel engines: A thermodynamic comparison between Kalina and ORC cycles," Appl. Therm. Eng., **30**(2-3), pp. 212–219.

[9] DiPippo, R., 2004, "Second Law assessment of binary plants generating power from low-temperature geothermal fluids," Geothermics, **33**(5), pp. 565–586.

[10] Walraven, D., Laenen, B., and D'Haeseleer, W., 2013, "Comparison of thermodynamic cycles for power production from low-temperature geothermal heat sources," Energy Convers. Manag., **66**, pp. 220–233.

[11] Singh, O. K., and Kaushik, S. C., 2013, "Energy and exergy analysis and optimization of Kalina cycle coupled with a coal fired steam power plant," Appl. Therm. Eng., **51**(1-2), pp. 787–800.

[12] Nguyen, T.-V., Knudsen, T., Larsen, U., and Haglind, F., 2014, "Thermodynamic evaluation of the Kalina split-cycle concepts for waste heat recovery applications," Energy, **71**, pp. 277–288.

[13] Shankar Ganesh, N., and Srinivas, T., 2012, "Design and modeling of low temperature solar thermal power station," Appl. Energy, **91**(1), pp. 180–186.

[14] Sun, F., Zhou, W., Ikegami, Y., Nakagami, K., and Su, X., 2014, "Energy-exergy analysis and optimization of the solar-boosted Kalina cycle system 11 (KCS-11)," Renew. Energy, **66**, pp. 268–279.

[15] Srinivas, T., and Reddy, B. V., 2014, "Thermal Optimization of a Solar Thermal Cooling Cogeneration Plant at Low Temperature Heat Recovery," J. Energy Resour. Technol., **136**(2), p. 021204.

[16] Madhawa Hettiarachchi, H. D., Golubovic, M., Worek, W. M., and Ikegami, Y., 2007, "The Performance of the Kalina Cycle System 11(KCS-11) With Low-Temperature Heat Sources," J. Energy Resour. Technol., **129**(3), p. 243.

[17] Arslan, O., 2011, "Power generation from medium temperature geothermal resources: ANN-based optimization of Kalina cycle system-34," Energy, **36**(5), pp. 2528–2534.

[18] Campos Rodríguez, C. E., Escobar Palacio, J. C., Venturini, O. J., Silva Lora, E. E., Cobas, V. M., Marques dos Santos, D., Lofrano Dotto, F. R., and Gialluca, V., 2013, "Exergetic and economic comparison of ORC and Kalina cycle for low temperature enhanced geothermal system in Brazil," Appl. Therm. Eng., **52**(1), pp. 109–119.

[19] Nag, P. K., and Gupta, a. V. S. S. K. S., 1998, "Exergy analysis of the Kalina cycle," Appl. Therm. Eng., **18**(6), pp. 427–439.

[20] Kim, K. H., Ko, H. J., and Kim, K., 2014, "Assessment of pinch point characteristics in heat exchangers and condensers of ammonia-water based power cycles," Appl. Energy, **113**, pp. 970–981.

[21] Determan, M. D., and Garimella, S., 2012, "Design, fabrication, and experimental demonstration of a microscale monolithic modular absorption heat pump," Appl. Therm. Eng., **47**, pp. 119–125.

[22] Delahanty, J. C., Garimella, S., and Garrabrant, M. A., 2015, "Design of compact microscale geometries for ammonia–water desorption," Sci. Technol. Built Environ., **21**(3), pp. 365–374.

[23] Keinath, C. M., Hoysall, D., Delahanty, J. C., Determan, M. D., and Garimella, S., 2015, "Experimental assessment of a compact branched tray generator for ammonia–water desorption," Sci. Technol. Built Environ., **21**(3), pp. 348–356.

[24] Fronk, B. M., and Garimella, S., 2013, "In-tube condensation of zeotropic fluid mixtures: A review," Int. J. Refrig., **36**(2), pp. 534–561.

[25] Fronk, B. M., and Garimella, S., 2016, "Condensation of ammonia and high-temperature-glide ammonia/water zeotropic mixtures in minichannels – Part I: Measurements," Int. J.

Heat Mass Transf., **in press**.

[26] Garimella, S., and Fronk, B. M., 2015, Encyclopedia of Two-Phase Heat Transfer and Flow I: Fundamentals and Methods Volume 2: Condensation Heat Transfer, World Scientific Publishing Co.

[27] Colburn, A. P., and Drew, T. B., 1937, "The condensation of mixed vapors," Transcations Am. Inst. Chem. Eng., **33**, pp. 197–215.

[28] Price, B., and Bell, K., 1973, "Design of binary vapor condensers using the Colburn-Drew equations," AIChE Symp. Ser., **70**(138), pp. 163–171.

[29] Jin, D. X., Kwon, J. T., and Kim, M. H., 2003, "Prediction of in-tube condensation heat transfer characteristics of binary refrigerant mixtures," Int. J. Refrig., **26**(5), pp. 593–600.

[30] Fronk, B. M., and Garimella, S., 2014, "Improved Non-Equilibrium Film Method for the Design of High-Temperature-Glide, Mini- and Microchannel Condensers," ASME 2014 International Mechanical Engineering Congress & Exposition, ASME, Montreal, Quebec, Canada.

[31] Cavallini, A., Censi, G., Del Col, D., Doretti, L., Longo, G. A., and Rossetto, L., 2002, "A tube-in-tube water/zeotropic mixture condenser: design procedure against experimental data," Exp. Therm. Fluid Sci., **25**(7), pp. 495–501.

[32] Silver, R. S., 1963, "An Approach to a General Theory of Surface Condensers," Proc. Inst. Mech. Eng., **178**(14), pp. 339–376.

[33] Bell, K. J., and Ghaly, M. A., 1973, "An approximate generalized design method for multicomponent/partial condenser," AIChE Symp. Ser., **69**(131), pp. 72–79.

[34] Del Col, D., Cavallini, a., and Thome, J. R., 2005, "Condensation of Zeotropic Mixtures in

Horizontal Tubes: New Simplified Heat Transfer Model Based on Flow Regimes," J. Heat Transfer, **127**(3), p. 221.

[35] Deng, H., Fernandino, M., and Dorao, C. A., 2014, "Numerical study of heat and mass transfer of binary mixtures condensation in mini-channels," Int. Commun. Heat Mass Transf., **58**, pp. 45–53.

[36] Deng, H., Fernandino, M., and Dorao, C. A., 2015, "Numerical Study of the Condensation Length of Binary Zeotropic Mixtures," Energy Procedia, **64**(1876), pp. 43–52.

[37] Lemmon, E. W., Huber, M. L., and McLinden, M. O., 2010, "REFPROP Reference Fluid Thermodynamic and Transport Properties - NIST Standard Reference Database 23, Version 9.0."

[38] Klein, S. A., 2014, "Engineering Equation Solver."

[39] Churchill, S., 1977, "Friction-Factor Equation Spans All Fluid-Flow Regimes," Chem. Eng., **84**(24), pp. 91–92.

[40] Fronk, B. M., and Garimella, S., 2016, "Condensation of ammonia and high-temperature-glide zeotropic ammonia/water mixtures in minichannels – Part II: Heat transfer models," Int. J. Heat Mass Transf., **in press**.

[41] Chilton, T. H., and Colburn, A. P., 1934, "Mass transfer (absorption) coefficients prediction from data on heat transfer and fluid friction," Ind. Eng. Chem., **26**(11), pp. 1183–1187.

[42] Dobson, M. K., and Chato, J. C., 1998, "Condensation in Smooth Horizontal Tubes," J. Heat Transfer, **120**(1), p. 193.

[43] Cavallini, A., Col, D. Del, Doretti, L., Matkovic, M., Rossetto, L., Zilio, C., and Censi, G., 2006, "Condensation in Horizontal Smooth Tubes: A New Heat Transfer Model for Heat

Exchanger Design," Heat Transf. Eng., **27**(8), pp. 31–38.

[44] Shah, M. M., 1979, "A General Correlation for Heat Transfer During Film Condensation inside Pipes," Int. J. Heat Mass Transf., **22**, pp. 547–556.

[45] Kim, S. M., and Mudawar, I., 2013, "Universal approach to predicting heat transfer coefficient for condensing mini/micro-channel flow," Int. J. Heat Mass Transf., **56**(1-2), pp. 238–250.

[46] Keinath, B. L., 2012, "Void Fraction, Pressure Drop and Heat Transfer in High Pressure Condensing Flows through Microchannels," Georgia Institute of Technology.

[47] Keinath, B. L., and Garimella, S., 2015, "Measurement and Modeling of Void Fraction in High Pressure Condensing Flows through Microchannels," Heat Transf. Eng., **accepted**.

[48] Heymann, D., Pence, D., and Narayanan, V., 2010, "Optimization of fractal-like branching microchannel heat sinks for single-phase flows," Int. J. Therm. Sci., **49**(8), pp. 1383–1393.

[49] Kwak, Y., Pence, D., Liburdy, J., and Narayanan, V., 2009, "Gas–liquid flows in a microscale fractal-like branching flow network," Int. J. Heat Fluid Flow, **30**(5), pp. 868–876.

[50] Kim, S. M., and Mudawar, I., 2012, "Universal approach to predicting two-phase frictional pressure drop for adiabatic and condensing mini/micro-channel flows," Int. J. Heat Mass Transf., **55**(11-12), pp. 3246–3261.

Figure Caption List

Table Caption List